Comprehensive analysis of laboratory boron contamination for boron isotope analyses of small carbonate samples

Kubota, Kaoru ; Ishikawa, Tsuyoshi ; Nagaishi, Kazuya ; Kawai, Tatsuya ; Sagawa, Takuya ; Ikehara, Minoru ; Yokoyama, Yusuke ; Yamazaki,…

(Citation)
Chemical Geology,576:120280

(Issue Date)
2021-08-20

(Resource Type)
journal article

(Version)
Accepted Manuscript

(URL)
https://hdl.handle.net/20.500.14094/90008414

Title:

Comprehensive analysis of laboratory boron contamination for boron isotope analyses of small carbonate samples

Author list:

Kaoru Kubota[1,2]

[1] Graduate School of Human Development and Environment, Kobe University

[2] Kochi Institute for Core Sample Research, Japan Agency for Marine-Earth Science and Technology (JAMSTEC)

Tsuyoshi Ishikawa[2],

[2] Kochi Institute for Core Sample Research, Japan Agency for Marine-Earth Science and Technology (JAMSTEC)

Kazuya Nagaishi[3]

[3] Marine Works Japan Ltd.

Tatsuya Kawai[3]

[3] Marine Works Japan Ltd.

Takuya Sagawa[4]

[4] Institute of Science and Engineering, Kanazawa University

Minoru Ikehara[5]

[5] Center for Advanced Marine Core Research, Kochi University

Yusuke Yokoyama[6]

[6] Atmosphere and Ocean Research Institute, The University of Tokyo

Toshitsugu Yamazaki[6]

[6] Atmosphere and Ocean Research Institute, The University of Tokyo

Corresponding author:
Kaoru Kubota
Graduate School of Human Development and Environment, Kobe University
3-11 Tsurukabuto, Nada-ku, Kobe, Japan, 657-8501
+81-078-803-7755 (Tel)
kaoryu0129@gmail.com

Abstract:

Boron isotopes are widely used as a proxy of marine carbonate in paleoclimatology to reconstruct seawater pH and atmospheric pCO_2, and precise and accurate boron isotopic analysis is required for this purpose. Determination of boron isotopic composition is susceptible to contamination, especially for sample analyses with small amounts of boron; however, sources of experimental and laboratory contamination are not clearly evaluated. In this study, boron and boron isotope contamination during the analysis of small carbonate samples were examined in detail during sample cleaning, sample storage, chemical separation, and isotope measurement. Repeated cleaning of foraminifera shells using H_2O with ultrasonication effectively minimized boron contamination from clay-rich material; however, an additional cleaning step with methanol and H_2O_2 is recommended to obtain repeatable precise $\delta^{11}B$, $\delta^{18}O$, and Mg/Ca values. Boron contamination during sample storage in a glass vial was far greater than expected. Glass-derived boron attached to foraminifera shells could not be completely removed by any physical or chemical cleaning process and influenced the $\delta^{11}B$ value significantly. Even when a low-boron HEPA, boron-free HEPA, or ULPA filter was used for air-handling in the laboratory, airborne contamination by gaseous boron can still be significant, with seasonal variation in abundance and isotopic composition. Although this affects the procedural blank of boron during chemical separation, an acid-removing chemical filter can reduce the airborne boron flux. An autosampler in the MC-ICPMS analysis might be an additional source of airborne boron contamination.

Keywords: boron isotope, foraminifera, contamination, procedural blank, paleoclimatology, geochemistry

1. Introduction

Boron isotopes are used as a proxy to estimate past seawater pH and atmospheric CO_2 concentrations from reef-building coral skeletons and planktonic foraminifera shells (e.g., Foster, 2008; Hönisch et al., 2009; Kubota et al., 2014; Chalk et al., 2017; Wu et al., 2018; Dyez et al., 2018) and are useful for studying mechanisms underlying calcification in corals and responses to ocean acidification (e.g., McCulloch et al., 2012; Allison et al., 2014; Tanaka et al., 2015; Georgiou et al., 2015; Kubota et al., 2017). The coral skeleton, made of aragonite crystal, can be used to reconstruct short-term climate variability due to its relatively fast growth rate (e.g., 1–2 cm per year for massive *Porites* corals) but is less suitable for long-term climate reconstruction owing to its susceptibility to post-depositional alterations. Planktonic foraminifera shells, which are made of calcite crystal and preserved in marine sediment, are effective for reconstructing long-term climate variability, although the temporal resolution is limited due to the low sedimentation rate and/or homogenization of sediments during bioturbation. Boron concentrations in reef-building coral skeletons and planktonic foraminifera shells are as low as 50 ppm and 5–10 ppm, respectively (Hemming and Hanson, 1992; Henehan et al., 2016), and the range of variation in the boron isotope ratio ($\delta^{11}B$) expected from glacial–interglacial seawater pH changes (0.1–0.2 pH units) is as small as 1–2‰. Thus, a small sample size for boron isotope analysis that maintains satisfactory precision (practically, <0.3‰ error) is crucial, particularly for studies based on foraminifera, according to sample availability. However, a reduction in the boron sample size increases susceptibility to boron contamination during experiments. Many potential sources of boron contamination have been suggested, including detrital and authigenic minerals attached to carbonates, the experimental apparatus, analytical reagents, and even air in the laboratory. Even in clean laboratories, substantial contamination can result from gaseous boron derived from high-efficiency particulate air (HEPA) filters and architectural materials containing borosilicate glass fibers (Rosner et al., 2005; Misra et al., 2014). Despite extensive efforts to ensure a low total procedural blank (in the range of picograms to nanograms) (e.g., see summary in Misra et al., 2014), little is known about boron contamination in the experimental environment. Thus, a comprehensive understanding of potential sources of contamination is essential for further reduction and stabilization of procedural boron blanks and for the improvement of high-precision isotope analyses of small amounts of boron in natural samples.

In this paper, we present a series of experiments aimed at thoroughly tracing laboratory boron contamination and its isotopic effects in the processes from sample cleaning, sample storage, and chemical separation to isotopic measurements, using a multiple-collector inductively coupled plasma mass spectrometer (MC-ICPMS). We also examine the effectiveness of cleaning protocols for planktonic foraminifera for obtaining reliable $\delta^{11}B$, Mg/Ca, and $\delta^{18}O$ values from the same batch of samples to improve our understanding of the seawater CO_2 system based on pH, temperature, and salinity. Based on the results of these experiments, we identify and quantify major sources of boron and boron isotopic contamination and discuss their impacts on $\delta^{11}B$ analyses related to paleo-pH and paleo-pCO_2 studies.

2. Material and methods

2.1. Laboratory environment

All experiments were carried out at the Kochi Core Center (KCC), Kochi, Japan, which consists of two main buildings (Buildings A and B). Foraminifera shells were cleaned within a common acid-resistant fume hood in Building B. All subsequent procedures (sample dissolution, major and trace element analyses, chemical separation of boron using ion exchange columns, and boron isotope measurement) were performed in a clean room in Building A (Clean Lab A: Fig. 1). Clean Lab A is divided into two rooms, the Preparation Room and the ICPMS Room, and air in both rooms passes through low-boron HEPA filters. The Preparation Room has a vertical laminar flow fume hood with air from a super ultra-low penetration air (ULPA) filter (hereafter, "clean fume hood") as well as a clean evaporator equipped with Teflon-coated hot plates and air from a boron-free super ULPA filter plus an acid-removing chemical filter. The air introduced into the clean fume hood and clean evaporator for filtering is ambient air in the laboratory. Clean Lab A was originally constructed in 2003 and was improved for boron isotope analysis in 2010 (including the replacement of filters in the clean air-handling system from normal HEPA to low-boron HEPA).

Another clean room was newly constructed in Building B (Clean Lab B) in late 2015. Clean Lab B has essentially the same clean air-handling system as that of Clean Lab A, except the air passes through boron-free HEPA filters, with no ICPMS room (Fig. 1). Clean Lab B was still under regulation in terms of the reduction of boron blanks throughout the study period, and data for airborne boron contamination were obtained in comparison with Clean Lab A.

2.2. Reagents and apparatus

All reagents and standard solutions were diluted in 18.2 MΩ·cm Milli-Q water (MQ; Merck Millipore, Burlington, MA). HCl, HNO_3, and HF used were all high-purity grade (TAMAPURE AA-100; Tama Chemicals, Kawasaki, Japan). A 1% (w/w) mannitol solution was prepared by dissolving D-mannitol (for the determination of boric acid; Merck, Darmstadt, Germany) in MQ. Analytical-grade 30% H_2O_2 (Fujifilm Wako Pure Chemical, Osaka, Japan), NaOH (analytical-grade; Sigma Aldrich, St. Louis, MO), and EL-grade methanol (Kanto Chemical Co., Tokyo, Japan) were used to clean foraminifera.

Teflon vials of 5, 7, and 15 mL (Savillex, Eden Prairie, MN) were cleaned with warm 6 M HNO_3 (3 days), MQ, warm 0.1 M HF (1 day), and MQ (three times), successively, before use.

2.3. Cleaning of foraminifera samples in marine sediment

A marine sediment core from the West Caroline Basin (0.10°S 139.58°E) collected by R/V Kairei in 2005 was used. The core included a 15-m-long piston core that covers the latest 400 ka (core KR05-15 PC01) and a 5-m-long pilot core taken by the Ewing-type pilot corer for a trigger (core KR05-15 PL01) (Yamazaki et al., 2005). The top 50 cm of the core, which covers the Holocene era (~11 thousand years ago to the present) and contains abundant planktonic foraminifera, was used. Sediment lithologies are foraminifera-rich clay (brown) in the top 30 cm and clay with foraminifera (greenish gray) in the lower part.

The sediment sample was cut at 2-cm intervals, gently washed under running water over a 63-µm sieve, and dried at 60°C in an oven. The materials from PC01 were stored in 5-mL polystyrene vials and those from PL01 were stored in 5-mL borosilicate glass vials. The sieved materials were then subdivided into fractions of 63–255, 255–300, 300–355, 355–425, 425–500, and 500–850 µm and stored in 5-mL polystyrene vials. Shells of *Trilobatus sacculifer* (60 mg each), previously recognized as *Globigerinoides sacculifer*, with a sac-like final chamber were hand-picked under a microscope from size fractions of 355–425 µm in the depth interval of 13–25 cm (7.3–10.8 thousand years ago) from PC01. *T. sacculifer* samples were stored in 1.5-mL polypropylene tubes and used for cleaning experiments. Additional samples of *Globigerinoides ruber* (300–355 µm) and *T. sacculifer* (500–850 µm, with sac-like chamber) were collected from PC01 and PL01 in a similar manner.

Samples of 60 mg of *T. sacculifer* shells were subdivided into 10 aliquots (6 mg each), and a suite of stepwise cleaning steps was performed. Then, in each cleaning procedure (referred to as Procedures A to J, Table 1), the cleaning process was stopped at different steps (Fig. 2, Fig. 3). These cleaning procedures for foraminifera shells are similar to those described in Barker *et al.* (2003), although those workers took a supernatant of the washing solution with suspended clays and fine silicates at each cleaning step and determined changes in trace element values (e.g., Mg/Ca). The full cleaning procedure (namely, Procedure J, Table 1) was as follows. After weighing, samples were crushed gently between two acrylic slides until the insides of all chambers were visible under a stereomicroscope (Fig. 2). Samples were then returned to 1.5-mL tubes and sonicated nine times with MQ water and twice with methanol. The supernatant containing suspended fine grains was removed immediately from the sample after ultrasonication. To remove organic matter by oxidation, 0.1 M-NaOH-buffered 30% H_2O_2 was added to the sample and heated at 80°C for 5 minutes, twice. Subsequent reductive steps described in Baker *et al.* (2003) were skipped in this study because they had no discernible effect on $\delta^{11}B$ (Ni et al., 2007; Misra et al., 2014). Finally, the sample was weakly acid-leached with 0.5 mM HCl to remove any adhesive materials attached to the calcium carbonate (e.g., detrital and authigenic minerals, foraminifera shell fragments, and coccolith).

The δ^{11}B, Mg/Ca, and δ^{18}O values for *Globigerinoides ruber* (300–355 μm) and *T. sacculifer* (500–850 μm) samples from PC01 after cleaning processes equivalent to Procedure I or J have been reported previously (Kubota et al., 2019).

2.4. Oxygen isotope analysis

An aliquot of several hundred micrograms of the cleaned foraminifera samples was taken for δ^{18}O analysis (Fig. 2). The oxygen isotope ratio was measured using an isotope-ratio mass spectrometer (Isoprime; Elementar, Cheadle Hulme, UK) and an automated carbonate reaction system (Multiprep, Elementar) (Fig. 2). The δ^{18}O values are reported with respect to the Vienna Pee Dee Belemnite standard (Craig, 1957). Analytical precision for long-term measurement of the calcite standard (IAEA603) was better than 0.1‰.

2.5. B/Ca, Mg/Ca, Al/Ca, Mn/Ca, and Ba/Ca analyses

The remaining cleaned foraminifera sample was transferred into a Teflon vial (Fig. 2). Then, 1 mL of 0.1 M HCl was added to the samples for complete dissolution, in addition to 5 μL of 1% mannitol solution. A 30-μL aliquot of the sample solution was diluted with 5 mL of 0.15 M HNO_3 with internal standards (50 ppb Be and 100 ppb Sc, Y, and In). First, the Ca concentration was measured using a quadrupole inductively coupled plasma mass spectrometer (Q-ICPMS; Agilent7700x, Agilent Technology, Santa Clara, CA). Then, another 30-μL aliquot of the sample solution was diluted similarly to give a Ca concentration of 10 ppm (matrix matching) (Fig. 2). Matrix matching is essential for the precise determination of trace element/Ca ratios (de Villiers et al., 2002; Sagawa et al., 2012). Using a standard solution (200 ppb of Mg and Sr, 50 ppb of B, Al, Mn, and Ba) prepared by diluting 1000 μg/g single element standards (SPEX CertiPrep, Metuchen, NJ) with the abovementioned internal standards, the B, Mg, Al, Mn, and Ba concentrations were determined using the Q-ICPMS (Fig. 2). A coral standard, JCp-1, provided by the Geological Survey of Japan, was repeatedly analyzed to estimate the precision of the trace element/Ca ratio measurements. The precision estimates for B/Ca, Mg/Ca, Al/Ca, Mn/Ca, and Ba/Ca analyses were 2.8%, 3.4%, 2.8%, 2.9%, and 2.5% (1σ), respectively. The errors for the estimated weights of $CaCO_3$ (mg) and boron (ng) in samples were 1.8% and 3.3%, respectively.

2.6. Boron isotope analysis

Techniques for chemical separation and isotope analyses of boron were previously described in Ishikawa and Nagaishi (2011) and Tanimizu *et al.* (2018). These methods constitute parts of the integrated analytical routine for boron and boron isotopes in KCC, in which HF-mannitol is commonly used for analyses of various types of samples, including fluids, carbonates, and silicate rocks (Nagaishi and Ishikawa, 2009; Yamaoka et al., 2012).

The sample dissolved in 0.1 M HCl after Q-ICPMS analysis was used for chemical purification (Fig. 2). Boron in the sample was chemically separated using successive cation- and anion-exchange resin columns (0.1 mL of AG 50W X12 and 0.03 mL of AG 1–X4, respectively; 200–400 mesh; Bio-Rad, Hercules, CA) with eluents of 0.1 M HCl, 0.5 M HF–2M HF, and 6 M HCl. The purified boron recovered by 0.15 mL of 6 M HCl was evaporated to dryness with mannitol at 45°C–60°C overnight. The sample was then dissolved with a "base solution" composed of 0.15 M HNO_3, 0.05 M HF, and 0.1% mannitol to obtain a solution of 20–75 ppb B. Then, a Li 1000 ppm solution (SPEX CertiPrep., Lot. 11-24Li) was added to the sample solution to obtain 100 ppb Li. At least 0.65 mL of the sample solution was used for a single run, and 13–50 ng of boron was consumed. The $\delta^{11}B$ value was determined using a MC-ICPMS (Neptune; Thermo Fisher Scientific, Dreieich, Germany) against the isotopic reference NIST-SRM 951 (Fig. 2). Mass-discrimination correction was performed by $^{7}Li/^{6}Li$ normalization in combination with a standard-sample bracketing technique (Tanimizu et al., 2018). A JET-sampling cone was used with an X-skimmer cone to increase sensitivity (He et al., 2016). $\delta^{11}B$ for JCp-1 determined for 20–75 ppb B solutions was 24.37 ± 0.22‰ (2σ, n = 11) The $\delta^{11}B$ values of AE122, boron isotopic reference material provided by Federal Institute for Materials Research and Testing (BAM), determined for 75 ppb B solution were 39.51 ± 0.24‰ (2σ, n = 4). These $\delta^{11}B$ values for JCp-1 and AE122 are consistent with the values obtained by a positive-ion thermal ionization mass spectrometer installed at KCC (P-TIMS; Ishikawa and Nagaishi, 2011; Tanimizu et al., 2018) and compiled values reported by Foster *et al.* (2010), Foster *et al*. (2013), and Gutjahr et al. (2020).

2.7. Evaluation of procedural boron contamination

2.7.1. Airborne boron contamination

From July 2017 to February 2020, airborne boron contamination within the clean room and equipment were monitored in Clean Lab A (Preparation Room) and in Clean Lab B. Boron in the air was collected over 24 h in an open 7-mL Teflon vial with 1 mL of base solution (0.15 M HNO_3, 0.05 M HF, and 0.1% mannitol). Monitoring was carried out on the lab table and inside the clean fume hood and clean evaporator. In Clean Lab B, monitoring on the lab table was performed at two different positions. The recovered vial was weighed to correct for mass loss due to evaporation during the exposure period, and then the boron concentration in the solution was determined by Q-ICPMS. Boron flux from the air was calculated (in picograms per hour per square centimeter). Similar exposure experiments were performed on the lab table of Clean Lab A in April 2010, in which the airborne boron contamination was evaluated before and after switching from normal HEPA to low-boron HEPA filters.

To understand boron isotope characteristics of air-derived boron, another suite of experiments was performed in the period between January 2019 and February 2020. Five open 15-mL Teflon vials with 5 mL of 0.1 M HCl and 0.002% mannitol solution were exposed for 10 days outside of the clean evaporator in Clean Lab A (Preparation Room). After drying at 60°C within the clean evaporator, 0.13 mL of the base solution was added to the vials, and all of the solutions were combined in a 5-mL V-shaped Teflon vial (0.65 mL in total). The δ^{11}B value of the solution was then measured using the MC-ICPMS.

2.7.2. Boron contamination during chemical purification

The total procedural blank of boron was monitored throughout sample dissolution, chemical separation, and the preparation of the final solution. To evaluate how the total procedural blank influences the measured δ^{11}B value of a carbonate sample when the sample size is small, diluted JCp-1 solutions with 5, 10, 15, 20, 30, 40, 50 ppb B were prepared from a laboratory stock solution with 200 ppb B. One milliliter of each solution was independently purified for boron and the δ^{11}B value was measured by MC-ICPMS analysis. This experiment was performed twice (July 2018 and January 2019).

2.7.3. Autosampler-derived boron contamination

In the MC-ICPMS analysis, the sample solution was handled using an autosampler (SC-micro DX; Elemental Scientific, Omaha, NE) covered with a custom-made plastic case enabling N_2 gas purge at a rate of 3 L/min. The sample vials were open and were exposed to air during δ^{11}B measurements, providing an opportunity for additional airborne boron contamination. We measured an airborne boron blank within the autosampler with and without N_2 gas purge, following similar methods to those described in Section 2-7-1. The δ^{11}B value for autosampler-air-derived boron was also measured. In this case, the Teflon vials with ca. 5 mL of base solution were left open for 65 h on the weekend (when the autosampler was stopped) or for 55 h on weekdays (when the autosampler was running) without N_2 gas purge. After reaching dryness at 60°C in a clean evaporator, 0.65 mL of the base solution was added to each vial, and the δ^{11}B values were measured by MC-ICPMS.

To understand how airborne boron contamination within the autosampler affects analyses of carbonate δ^{11}B, a purified JCp-1 solution (20 ppb B) was analyzed continuously without N_2 gas purge for 4.5 h or for 6 h. The time-dependent shift in observed δ^{11}B values was monitored.

3. Results and Discussion

3.1. Influence of sediment-derived contamination

The results of step-wise cleaning experiments are summarized in Fig. 3. After successive steps to remove detrital and authigenic minerals and shell fragments from foraminifera shells, the weight of $CaCO_3$ decreased to one-third of the original weight (4–5 mg) (Fig. 3a). Procedure C (ultrasonication and supernatant removal in MQ, repeated three times) caused a loss of nearly half of the $CaCO_3$. The B/Ca ratio, initially 110 µmol/mol, also decreased substantially to 80 µmol/mol during Procedure C and was constant thereafter (Fig. 3b). The weight of boron in the sample showed a similar trend. The $\delta^{11}B$ value was initially 15.5‰, increased rapidly to 19‰ during cleaning with MQ, and did not change substantially thereafter (Fig. 3c). Organic matter removal using H_2O_2 (Procedures H and I, Table 1) did not affect the $\delta^{11}B$ value.

There was an inverse correlation between B/Ca and $\delta^{11}B$ during cleaning, indicating the removal of the boron-rich, low-$\delta^{11}B$ component. Cross-plots of $\delta^{11}B$ versus B/Ca and Ca/B showed a clear mixing relationship, and the contribution of a boron-rich end-component with $\delta^{11}B$ = ~8‰, was predicted (Fig. 4). This end-component $\delta^{11}B$ value is consistent with those of authigenic marine minerals, such as smectite-series clay and silica, rather than detrital illite-rich clay with very low $\delta^{11}B$ values of less than −5‰ (Ishikawa and Nakamura, 1993). Because authigenic sedimentary minerals and detritus show distinctly lower $\delta^{11}B$ values compared with those of planktonic foraminifera (19–22‰) (Henehan et al., 2016), the effects of such contaminants must be carefully examined, especially for samples with any diagenetic signature.

Although ultrasonication with MQ was sufficient for B/Ca and $\delta^{11}B$ analyses of foraminifera samples (Fig. 3b,c), the cleaning protocol must also be satisfactory for Mg/Ca and $\delta^{18}O$ analyses to obtain precise estimates of water temperature and salinity in addition to seawater pH. The Mg/Ca ratio decreased dramatically by cleaning with MQ (Fig. 3e). However, organic matter removal using H_2O_2 further decreased the Mg/Ca ratio by 0.3 mmol/mol, which is significant considering the analytical error of 0.14 mmol/mol. The Al/Ca and Ba/Ca ratios (and to a lesser extent the Mn/Ca ratio) showed similar responses to those of Mg/Ca (Fig. 3f,g,h). This is expected if the contaminants contain clays enriched in Mg, Al, and Ba. Therefore, as previously suggested, Al/Ca is a useful indicator of insufficient clay removal from foraminifera shells (e.g., Baker *et al.*, 2003; Ni et al., 2007; Chalk et al., 2017), as is Ba/Ca. The shell $\delta^{18}O$ values decreased slightly by 0.3‰ during cleaning, although the observed decrease was generally within the analytical error (Fig. 3d). Possible explanations for a small $\delta^{18}O$ shift have been discussed previously (e.g., Hönisch and Hemming, 2004; Ni *et al*., 2007; Kubota *et al.*, 2019). Irrespective of the mechanism, changes in $\delta^{18}O$ values were negligible.

Based on these results, we recommend the cleaning protocol represented by Procedure I or J (Table 1 and Fig. 3) for combined analyses of foraminiferal $\delta^{11}B$, Mg/Ca, and $\delta^{18}O$ together with Al/Ca and Ba/Ca screening to exclude clay-contaminated samples.

3.2. Boron contamination during sample storage

The $\delta^{11}B$ values determined for *G. ruber* (300–355 µm) and *T. sacculifer* (500–850 µm) collected from the pilot core PL01 and cleaned by Procedure J are shown in Fig. 5, along with previously reported data for the piston core PC01 (Kubota et al., 2019). The $\delta^{11}B$ values obtained for PL01 were distinctly lower with greater scatter compared with values for PC01 in any given age period, whereas B/Ca, Mg/Ca, Ba/Ca, $\delta^{18}O$ estimates for the two sets of samples were consistent (Supplementary Figures S1 and S2). SEM analyses did not show notable differences in the degree of shell dissolution between PC01 and PL01 or secondary calcite precipitation, which may affect parameter estimates (e.g., Sexton et al., 2016). The $\delta^{11}B$ values for *G. ruber* and *T. sacculifer* reported for the western equatorial Pacific marine sediment (ODP 806B, Foster, 2008) are consistent with those for PC01 (Fig. 5), and thus the $\delta^{11}B$ values observed for PL01 were clearly anomalous. As mentioned earlier, the only difference between the PL01 and PC01 samples is that the washed materials were initially stored in borosilicate glass vials in the case of PL01 and in polystyrene vials for PC01. This strongly suggests that the systematically lower $\delta^{11}B$ values by 1–2‰ observed for PL01 resulted from boron contamination from sample vials made of borosilicate glass (which contains 11.0% B_2O_3, or 3.5% B).

To identify the $\delta^{11}B$ value for glass-originated boron, we leached 5-mL borosilicate glass vials, the same type used for PL01, with 4.5 mL of 0.1 M HCl for 90 h at room temperature. The resultant leachate showed a $\delta^{11}B$ value of −5.4‰. Taking this $\delta^{11}B$ value and 3.5% B for the glass, the estimated weight of contaminant glass required for a decrease in $\delta^{11}B$ of 1‰ for a 3-mg foraminifera sample (ca. 25 ng of B) is only 3.2×10^{-5} mg (1.1 ng of B). Because this is only 1/25 of the boron in the original foraminifera shell, it is difficult to interpret such boron contamination as a subtle increase in the B/Ca ratio of the sample. For instance, the contamination increases the B/Ca ratio from 100 to 104 µmol/mol, within the analytical uncertainty (ca. 6 µmol/mol). The extremely low contaminant/sample weight ratio (ca. 1×10^{-5}) makes it impossible to detect contamination by other parameters, including Mg/Ca, Al/Ca, and Ba/Ca. Thus, the glass-derived contamination selectively affects $\delta^{11}B$ without producing any detectable anomalies in other parameters, as confirmed in PL01 (Fig. 5).

Of note, the glass vial was used only for temporary storage of the >63 µm fraction of sediment samples containing foraminifera shells and glass-derived boron contamination was nevertheless observed for all foraminifera samples for PL01. This indicates that very fine particles of glass attached to foraminifera shells by mechanical scraping cannot be removed completely by physical or chemical cleaning processes, like those shown in Fig. 3. Additionally, boron in such glass particles can be effectively leached out during dissolution of the sample using 0.1 M HCl; the leachate contained 1150 ppb B. Although the potential for serious boron contamination from glassware is well-established, we further conclude that the storage of samples for $\delta^{11}B$ paleo-pH and paleo-pCO_2 studies in borosilicate glass vials must be avoided, even for short durations.

3.3. Laboratory airborne boron contamination

The results of long-term analysis (spanning 2.5 years in 2017–2020) of laboratory airborne boron contamination are summarized in Figs. 1 and 6. Clean Lab A, where the chemical separation of boron and Q-ICPMS and MC-ICPMS analyses were performed, showed average airborne boron fluxes of 0.0–10.9 pg/h/cm^2 on the lab table and 1.1–31.3 and 0.0–1.9 pg/h/cm^2 within the clean fume hood and clean evaporator, respectively (Supplementary Table 1). Clean Lab B, which was not set up as a boron isotope analytical environment, showed average airborne boron fluxes of 0.5–31.4, 0.0–16.6, and 0.2–29.7 pg/h/cm^2 for the lab table, clean fume hood, and clean evaporator, respectively. In earlier experiments on the lab table of Clean Lab A in April 2010, average airborne boron fluxes were 13.0 and 0.7 pg/h/cm^2 before and after the replacement of air-handling filters from normal HEPA to low-boron HEPA, respectively. Some relevant features of the laboratory environments should be pointed out.

(1) There was clear seasonality in airborne boron fluxes in both Clean Labs A and B. The fluxes were particularly high in the summer and relatively low in the winter (Fig. 6). For example, the boron fluxes on the lab table of Clean Lab A were 5.3–10.9 pg/h/cm^2 in May–August and 0.0–2.0 pg/h/cm^2 in other months. In addition, the airborne boron fluxes on the lab tables and inside the clean fume hoods of Clean Labs A and B vary synchronously (Fig. 6a,b). Because room temperature remained relatively constant, season-dependent airborne boron contamination generated inside the lab is unlikely. The synchronous variation in labs in different buildings suggests that the source of airborne boron is outside of the clean labs.

(2) As shown previously (Rosner et al., 2005; Misra et al., 2014), glass fiber-containing normal HEPA filters cause significant airborne boron contamination. This was confirmed by the exceedingly higher boron flux with normal HEPA (13.0 pg/h/cm^2) compared with low-boron HEPA (0.7 pg/h/cm^2) observed in Clean Lab A. However, boron-free HEPA (Clean Lab B) and super ULPA (clean fume hood in both labs) did not further reduce airborne boron beyond that for the low-boron HEPA (Clean Lab A). This clearly indicates that the form of airborne boron is not particulate but gaseous, and this issue cannot be resolved by boron-free HEPA or super ULPA. However, the airborne boron flux within the clean evaporator in Clean Lab A remained very low (Fig. 6c), indicating that gaseous boron was efficiently reduced by the acid-removing chemical filter attached to the apparatus.

(3) In Clean Lab B, anomalously high airborne boron fluxes (9.0–30.2 pg/h/cm^2) in February 2020, a

winter month (Fig. 6a), could be attributed to a slight leak of non-filtered air into Clean Lab B (an increase of <0.3 μm particles was observed). High, scattered airborne boron fluxes within the clean evaporator of Clean Lab B until July 2019 (Fig. 6c) were due to insufficient cleaning of inner pipes connecting the filter unit to the evaporation chambers. After cleaning with H_2O in July 2019, the airborne boron fluxes decreased and remained relatively low, even when the abovementioned leak of non-filtered air occurred in February 2020. Thus, the strict control of the air-handling system and the thorough cleaning of the experimental apparatus are particularly important for maintaining low airborne-boron conditions.

Another suite of exposure experiments showed clear seasonality in δ^{11}B values for airborne boron in Clean Lab A (Fig. 7), which was negatively correlated with the airborne boron flux ($r = -0.81$, $p < 0.05$, $N = 11$). The elevated airborne boron fluxes in the summer were accompanied by low δ^{11}B values of −3‰ to −1‰, and the δ^{11}B values increased up to 12‰ as the airborne born flux decreased in the winter. This suggests that the sources of airborne boron differ between the summer and winter.

The seasonality of laboratory airborne boron and boron isotope fluxes has not been reported in the literature to date. The seasonal variation in both airborne boron and δ^{11}B was apparently correlated with the outside temperature and precipitation (Fig. 7), implying that the parameters are determined by meteorological factors. The majority of boron (>90%) exists in the atmosphere in gaseous form (Fogg and Duce, 1985), the major sources of which are coal combustion, seawater, and volcanic emission (Fogg and Duce, 1985; Miyata et al., 2000). The δ^{11}B values for airborne boron observed during the winter and spring (7–12‰) are consistent with a mixture of coal-burning-derived boron and seawater boron transported from the Asian continent and the Japan Sea by the NW prevailing wind in these seasons (Sakata et al., 2010). However, we cannot identify a likely source for the airborne boron with a low δ^{11}B value in the summer (−3‰ to −1‰). Although the KCC is located near the Pacific coast, the low δ^{11}B signature is unlikely to be derived from the sea, even if complicated isotopic fractionation of boron during seawater evaporation is considered (Xiao et al., 2007). Anthropogenic sources of boron, especially from agricultural activities, such as the cultivation of rice and burning of biomass by farmers near KCC, may explain relatively low δ^{11}B estimates (−2‰ to 15‰: Komor, 1997). It is also not possible to rule out the existence of an unidentified boron source containing borosilicate glass fibers outside of the clean lab (such as flame-retardant and heat-insulating materials in the building, which can show δ^{11}B <0‰, similar to borosilicate glass vials, as discussed in Section 3-2). Exposure to hot, humid air in the summer might promote the production of airborne boron with a low-δ^{11}B signature by these materials.

Hence, although we recommend the use of low-boron HEPA, boron-free HEPA, or ULPA filters, laboratory airborne boron fluxes of external gaseous origin with seasonal variation can still be significant. Careful monitoring of airborne fluxes of boron and boron isotopes throughout the season is important, especially for δ^{11}B analyses with small sample sizes.

3.4. Influence of the procedural boron blank on δ^{11}B analyses

The total procedural blanks of boron, throughout sample dissolution, chemical separation, and final evaporation, in the study period are shown in Fig. 8a. The observed boron blanks varied between 43 pg and 480 pg. From February to June, the majority of blank were within 43–120 pg; after late April, larger blanks ranging from 200 to 480 pg appeared (Fig. 8a). Reagent blanks of boron for MQ, TAMAPURE 30% HCl, and 38% HF were 0.013, 0.16, and 0.044 ppb, respectively. Based on these data, the total reagent blank of boron throughout the above procedures was 43 pg. Some total procedural blanks in February and March were nearly identical to the estimated total reagent blank. However, total procedural blanks exceeding 50 pg indicate an additional boron source. Considering the seasonality, airborne boron is the most likely source. In the worst case (480 pg of B in late July), 90% of boron in the total procedural blank was likely derived from airborne contamination.

As mentioned earlier, the airborne boron flux within the clean evaporator of Clean Lab A, where the evaporation of sample solutions was performed, was as low as 0.0–1.9 pg/h/cm^2 due to the acid-removing chemical filter (Fig. 6c). Although the purified sample was maintained in 0.15 mL of 6 M HCl overnight for evaporation, the surface area of the solution was only $\leq$0.4 cm^2 and therefore the airborne boron contamination was minimal, probably <5 pg. However, the entrainment of airborne boron during chemical separation is not straightforward because the column and vial were covered with a plastic case to prevent exposure to the ambient air flow, except when the sample solution and eluents were added to the column. Chemical separation was performed on the lab table or within the clean fume hood of Clean Lab A and the full procedure, from the preparation and cleaning of the columns to final recovery of the purified boron sample, required about 9 h. The maximum airborne boron flux was approximately 10–30 pg/h/cm^2 (Figs. 6a,b and 7a); thus, over a 9-h period, airborne boron contamination of 90–270 pg/cm^2 is expected. Although it is difficult to estimate the effective surface area, airborne contamination during chemical separation is likely to explain the increase in the total procedural blank of boron.

Given the substantial variation in the procedural boron blank, its influence on δ^{11}B measurements must be evaluated. Here, seasonal variation in the procedural boron blank and its δ^{11}B value were approximated as sinusoidal curves that have maximum values in August and February, respectively (Fig. 8a), assuming that the boron blank is largely of airborne origin. Based on these curves, we estimated the influence of the blank on boron isotope measurements of calcium carbonate with the coral standard JCp-1 (Fig. 8b). When the sample size of boron is larger than 40 ng, the influence of the blank is expected to be within the analytical uncertainty throughout the year. However, for <40 ng of B, the effect can exceed the analytical uncertainty, especially during the summer.

Actual measurements of JCp-1, for which samples with 5–50 ng of B were independently purified, were consistent with this prediction (Fig. 8c). When the total procedural boron blank was as low as 56 pg (January 2019), there was no significant difference between the δ^{11}B values obtained for various boron amounts, indicating that the influence of the procedural blank is negligible, even when the boron sample size was as low as 5 ng. For the boron blank with 476 pg (July 2018), the δ^{11}B measurements on JCp-1 with 10 and 20 ng of boron showed low values, consistent with the expectation based on the model. Because the typical boron blank in our lab was 50–300 pg, the minimum amount of boron necessary to obtain precise δ^{11}B values is 40 ng, as estimated based on the boron blank.

Thus, to minimize the influence of the procedural blank on δ^{11}B analyses with small sample sizes, it is important to reduce and monitor airborne boron contamination. This is clearly evidenced by our ability to measure the δ^{11}B values for small samples precisely when the airborne boron flux was low and the total procedural blank was nearly identical to the total reagent blank (Figs. 6–8). An effective use of an acid-removing chemical filter may help. The use of the micro-distillation method (Misra et al., 2014; McCulloch et al., 2014; Raitzsch et al., 2018), depending on the type of analyte, might also be effective.

3.5. Boron contamination from the MC-ICPMS autosampler

Airborne boron fluxes observed in the MC-ICPMS autosampler with and without N_2 purge were 32.8 and 14.5–275 pg/h/cm^2, respectively. The δ^{11}B values for airborne boron in the autosampler determined in October 2018 were 9.2‰, on average, and were 8.9‰ and 9.4‰ with boron fluxes of 70 and 67 pg/h/cm^2 when the autosampler was stopped, and 9.3‰ and 9.0‰ with boron fluxes of 78 and 98 pg/h/cm^2 when it was running. Such airborne boron contamination is avoidable when samples are analyzed individually without using an autosampler. However, when high-throughput analysis using an autosampler is required, this additional airborne contamination must be considered.

The results of successive δ^{11}B analyses of JCp-1 (20 ppb B) using the autosampler without N_2 purge are shown in Fig. 9. As time elapsed, the observed δ^{11}B value became low and deviated from the values of JCp-1 with 75 ppb B, beyond the analytical uncertainty, after 3 h. A simple two end-member mixing model assuming a δ^{11}B value of 9.2‰ and an average flux of 88 pg/h/cm^2 for airborne boron in the autosampler effectively explains the trend observed in δ^{11}B values for JCp-1 at 20 ppb B (dashed line in Fig. 9). The accumulation of airborne boron reached 700 pg at 3.5 h after the start of the experiment. N_2 purge can reduce the boron flux to 33 pg/h/cm^2, and the δ^{11}B analysis with 20 ppb B gives reliable results for 9.5 h.

The airborne boron fluxes observed in the autosampler were much higher than those obtained on the lab table of Clean Lab A (0.0–10.9 pg/h/cm^2), suggesting that there was a significant boron source inside the autosampler. This can be a small glass-made part, adhesive, or lubricant; these boron-containing materials can react to acid vapor to generate gaseous boron. The magnitude of the effect may depend on the model and type of autosampler. The HF solution, as used in this study, effectively washes the boron memory in the sample introduction system of MC-ICPMS (Misra et al., 2014; Tanimizu et al., 2018). However, we recommend special care and monitoring for airborne boron contamination during analyses using an autosampler because HF vapor easily reacts with boron-containing materials to produce gaseous BF_3.

4. Conclusions

We performed detailed evaluations of boron and boron isotope contamination during sample cleaning and storage, the chemical separation of boron, and $\delta^{11}B$ measurements for small carbonate samples. The important results and their implications can be summarized as follows:

(1) Repeated cleaning of foraminifera shells using H_2O with ultrasonication efficiently reduces boron contamination from clay-rich materials and thus yields satisfactory results for $\delta^{11}B$ analysis. However, additional successive cleaning using methanol and H_2O_2 is recommended to obtain precise Mg/Ca and $\delta^{18}O$ values. Al/Ca and Ba/Ca values are useful for screening clay-contaminated samples.

(2) When sediment samples are stored in borosilicate glass vials, perhaps fine particles of glass attach to foraminifera shells and cannot be removed completely by any physical or chemical cleaning process. Such glass-derived boron contamination can lower the observed $\delta^{11}B$ value for foraminifera samples by a few per mil with no detectable changes in B/Ca, Mg/Ca, Al/Ca, Ba/Ca, and $\delta^{18}O$ values. Thus, sample storage in a glass vial must be avoided, even over short periods.

(3) Even if a low-boron HEPA, boron-free HEPA, or ULPA filter is used in the lab, the airborne fluxes of gaseous boron and boron isotopes can still be significant and may exhibit large seasonal variation associated with meteorological factors peculiar to each lab worldwide. Within an experimental space with a relatively low rate of air flow, the use of an acid-removing chemical filter effectively reduces this airborne boron flux. The careful maintenance of air-handling systems and thorough cleaning of the experimental apparatus are essential to maintain low airborne boron.

(4) The total procedural blank of boron during chemical separation could be reduced to the expected level from the reagent blanks when the airborne boron flux in the lab was low. However, the total procedural blank tended to increase rapidly as the airborne boron flux increases, overwhelming the blank from reagents. Because such airborne boron contamination can lower the observed $\delta^{11}B$ value at the per-mil level, it is essential to monitor the airborne boron flux and procedural blank of boron for precise $\delta^{11}B$ analysis in small sample sizes.

(5) An autosampler in MC-ICPMS can provide an additional source of airborne boron contamination. This likely results from the reaction of acid vapor with components of the autosampler. Although the N_2 purge is effective at reducing this contamination, sample solutions should not be left for hours in $\delta^{11}B$ analyses of small samples, especially when an HF solution is used.

All types of contamination described above can readily result in a lower $\delta^{11}B$ value by several per mil than the true value for the marine carbonate samples. The reduction of these sources of contamination is essential for paleo-climate and paleo-environmental studies using carbonate boron isotope as seawater pH and $p\mathrm{CO}_2$ proxies.

Figure legends

Fig. 1. Schematics of the laboratory environments of Clean Labs A and B in KCC, together with boron fluxes observed on the lab tables and inside the devices (clean fume hood, clean evaporator, and autosampler of MC-ICPMS).

Fig. 2. Schematics of the experimental procedures for $\delta^{18}O$, Mg/Ca, and $\delta^{11}B$ measurements of foraminiferal samples.

Fig. 3. Results of stepwise cleaning of *T. sacculifer* shells collected from the Holocene section of KR05-15 PC01.

Fig. 4. (**a**) A cross-plot of $\delta^{11}B$ versus B/Ca of *T. sacculifer* shells during the stepwise cleaning experiment. Solid curve represents mixing with a contaminant with a $\delta^{11}B$ of 8‰. (**b**) Plot described in (a), but with Ca/B on the horizontal axis for a better presentation of the mixing relationship.

Fig. 5. A time-series of $\delta^{11}B$ values of (**a**) *G. ruber* and (**b**) *T. sacculifer* collected from KR05-15 PC01 (closed rectangles) and PL01 (open rectangles) during the Holocene. The $\delta^{11}B$ values for foraminifera reported in a sediment core of the Ontong-Java Plateau in the western equatorial Pacific (ODP 806B; 0.32°N, 59.37°E, Foster, 2008) are also shown (light blue crosses). It is a core top data from the depth 12–17, corresponding to 7300–8600 cal. yr BP. Note that *G. ruber* and *T. sacculifer* from PL01 show distinctly lower and more highly scattered $\delta^{11}B$ values compared with those from PC01 and ODP806B.

Fig. 6. Measured airborne boron fluxes since July 2017 (**a**) on the lab table, (**b**) inside the clean fume hood, and (**c**) inside the clean evaporator in Clean Labs A and B. In Clean Lab B, the boron fluxes were monitored at two different positions on the lab tables. Exceptionally high boron fluxes observed on the lab table in Clean Lab B in February 2020 were due to a leak of non-filtered air. High boron fluxes observed inside the clean evaporator in Clean Lab B until June 2019 were likely derived from dirt remaining inside the apparatus.

Fig. 7. (**a**) Airborne boron fluxes (black circles) and $\delta^{11}B$ values (red squares) in Clean Lab A monitored between January 2019 and February 2020. (**b**) Monthly mean air temperatures (orange circles) and monthly precipitation (blue triangles) during the same period observed at the Nankoku-nissho station (Kochi

Airport) near KCC (data provided by the Meteorological Agency of Japan, available at https://www.data.jma.go.jp/obd/stats/etrn/index).

Fig. 8. (**a**) Total procedural boron blanks (light blue diamonds) observed between February 2018 and February 2020 together with modeled seasonal variation in boron blanks (blue circles) and $\delta^{11}B$ values (black circles). (**b**) Calculated $\delta^{11}B$ values for JCp-1 with 10, 20, 30, 40, and 50 ng of B affected by season-dependent boron blanks. Horizontal line with gray shaded area represents a $\delta^{11}B$ value for blank-free JCp-1 (24.35 ± 0.22‰). (**c**) Observed influence of total procedural boron blanks (476 pg and 56 pg on July 2018 and January 2019, respectively) on the $\delta^{11}B$ values for JCp-1 with various boron sample sizes. Dashed lines represent calculated $\delta^{11}B$ values for blank-affected JCp-1 when the total procedural boron blanks are 100, 300, 500, and 1000 pg. The $\delta^{11}B$ values assumed for contaminants are −2.7‰ in July (orange) and 12.2‰ in January (blue).

Fig. 9. Influence of autosampler-derived airborne boron contamination on successive $\delta^{11}B$ measurements of the JCp-1 solution with 20 ppb B. Horizontal line with a gray shaded area represents a $\delta^{11}B$ value for blank-free JCp-1 (24.35 ± 0.22‰). Dashed line represents a mixing model assuming a boron flux of 88 pg/h/cm^2 and a $\delta^{11}B$ value of 9.2‰ for airborne boron contamination.

Acknowledgements

We obtained sediment samples from a repository of core samples maintained by JAMSTEC (http://www.jamstec.go.jp/kochi/jc_curation/e/index.html). We would like to thank N. Ahagon for core curation and assistance in sediment core sampling; H. Takagi for assistance in planktonic foraminifera picking; Y. Nagaiwa and N. Asakura for laboratory management; and T. Matsuzaki, Y. Fujimura, and T. Komatsu for technical support in $\delta^{18}O$ analysis. This study was financially supported by Research Fellowships for Young Scientists from the Japan Society for the Promotion of Science (JSPS) to K.K. (Grant Number: 17J04576); JSPS Kakenhi grants to K.K. (Grant Number: 18K18186), T.I. (Grant Numbers: 16H04066 and 21H01194), and T.S. (Grant Number: 15K21221); and a Grant for Environmental Research Projects from The Sumitomo Foundation to T.S. (Grant Number: 133303). Finally, we declare no competing interests. Finally, we are grateful to the two anonymous reviewers, whose comments substantially improved this manuscript.

References

Allison, N., Cohen, I., Finch, A. A., Erez, J., Tudhope, A. W., 2014. Corals concentrate dissolved inorganic carbon to facilitate calcification. Nat. commun. 5, 5741.

Bahr, A., Schönfeld, J., Hoffmann, J., Voigt, S., Aurahs, R., Kucera, M., Flögel, S., Jentzen, A., Gerdes, A., 2013. Comparison of Ba/Ca and $\delta^{18}O_{WATER}$ as freshwater proxies: A multi-species core-top study on planktonic foraminifera from the vicinity of the Orinoco River mouth. Earth Planet. Sci. Let. 383, 45–57.

Barker, S., Greaves, M., Elderfield, H., 2003. A study of cleaning procedures used for foraminiferal Mg/Ca paleothermometry. Geochem. Geophys. Geosyst. 4, https://dx.doi. org/10.1029/2003GC000559.

Be, A. W. H., 1980. Gametogeniccalcification in a spinose planktonic foraminifera, *Globigerinoides sacculifer* (Brady). Mar. Micropaleontol. 5, 283–310.

Chalk, T. B., Hain, M. P., Foster, G. L., Rohling, E. J., Sexton, P. F., Badger, M. P. S., Cherry, S. G., Hasenfratz, A. P., Haug, 20 G. H., Jaccard, S. L., Martínez-García, A., Pälike, H., Pancost, R. D. and Wilson, P. A., 2017. Causes of ice age intensification across the Mid-Pleistocene Transition. Proc. Nat. Acad. Sci. USA, 114(50), 13114–13119.

Chetelat, B., Gaillardet, J., Freydier, R., Negrel, Ph, 2005. Boron isotopes in precipitation: experimental constraints and field evidence from French Guiana. Earth Planet. Sci. Lett. 235, 16–30.

Craig, H., 1957. Isotopic standards for carbon and oxygen and correction factors for mass-spectrometric analysis of carbon dioxide. Geochim. Cosmochim. Acta 12, 133–149.

Dyez, K. A., Hönisch, B., Schmidt, G. A., 2018. Early Pleistocene obliquity‐scale pCO_2 variability at ~1.5 million years ago. Paleoceanogr. Paleoclimatol. 33(11), 1270–1291.

Fogg, T. R., Duce, R. A., 1985. Boron in the troposphere: distribution and fluxes. J. Geophys. Res. 90, 3781–3796.

Fogg, T. R., Duce, R. A., Fasching, J. L., 1983. Sampling and determination of boron in the atmosphere. Anal. Chem. 55(13), 2179–2184.

Foster, G. L., 2008. Seawater pH, pCO_2 and $[CO_3^{2-}]$ variations in the Caribbean Sea over the last 130 kyr: A boron isotope and B/Ca study of planktic foraminifera. Earth Planet. Sci. Lett. 271, 254–266.

Foster, G. L., Hönisch, B., Paris, G., Dwyer, G. S., Rae, J. W. B., Elliott, T. R., Gaillardet, J., Hemming, N. G., Louvat, P., Vengosh, A., 2013. Interlaboratory comparison of boron isotope analyses of boric acid, seawater and marine $CaCO_3$ by MC-ICPMS and NTIMS. Chem. Geol. 358, 1–14.

Foster, G. L., Pogge von Strandmann, P. A. E., Rae, J. W. B., 2010. Boron and magnesium isotopic composition of seawater. Geochem. Geophys. Geosys. 11, Q08015.

Georgiou L., Falter J., Trotter J., Kline D.I., Holcomb M., Dove S.G., Hoegh-Guldberg O.H., McCulloch

M., 2015. pH homeostasis during coral calcification in a free ocean CO_2 enrichment (FOCE) experiment, Heron Island reef flat, Great Barrier Reef. Proc. Natl. Acad. Sci. 112, 13219−13224.

Gray, W. R., Rae, J. W., Wills, R. C., Shevenell, A. E., Taylor, B., Burke, A., Gavin, G. L., Lear, C. H., 2018. Deglacial upwelling, productivity and CO_2 outgassing in the North Pacific Ocean. Nat. Geosci. 11(5), 340–344.

Gutjahr M., Bordier L., Douville E., Farmer J., Foster G. L., Hathorne E. C., Hönisch B., Lemarchand D., Louvat P., McCulloch M., Noireaux J., Pallavicini N., Rae J. W. B., Rodushkin I., Roux P., Stewart J. A., Thil F., You C. F., 2020. Sub-permil interlaboratory consistency for solution-based boron isotope analyses on marine carbonates. Geostand. Geoanal. Res. 41, 90–17.

He, M., Jin, Z., Lu, H., Deng, L., Luo, C., 2016. The different cones combination enhanced sensitivity on MC-ICP-MS: The results from boron isotope analysis. International J. Mass Spectrom. 408, 33–37.

Hemming, N. G., Hanson, G. N., 1992. Boron isotopic composition and concentration in modern marine carbonates. Geochim. Cosmochim. Acta 56(1), 537–543.

Henehan, M. J., Foster, G. L., Bostock, H. C., Greenop, R., Marshall, B. J., Wilson, P. A., 2016. A new boron isotope-pH calibration for *Orbulina universa*, with implications for understanding and accounting for ‘vital effects’. Earth Planet. Sci. Let. 454, 282–292.

Honisch, B., Hemming, N. G., 2004. Ground-truthing the boron isotope-paleo-pH proxy in planktonic foraminifera shells: Partial dissolution and shell size effects. Paleoceanogr. 19, PA4010, https://dx.doi.org/10.1029/2004PA001026.

Horrocks, A. R., Price, D., 2001 (Eds.). Fire retardant materials. Woodhead Publishing, Cambridge.

Hunt, C. D., 2002. Specific Boron-binding biomolecules. In: Goldbach, H. E., Rerkasem, B., Wilmmer, M. A., Brown, P. H., Thellier, M., Bell, R. W. (Eds.), Boron in Plant and Animal Nutrition. Springer Science, New York, https://dx.doi.org/10.1007/978-1-4615-0607-2.

Hönisch, B., Allen, K. A., Russell, A. D., Eggins, S. M., Bijma, J., Spero, H. J., Lea, D. W., Yu, J., 2011. Planktic foraminifers as recorders of seawater Ba/Ca. Mar. Micropaleontol. 79(1-2), 52–57.

Hönisch, B., Hemming, N. G., Archer, D., Siddall, M., McManus, J. F., 2009. Atmospheric carbon dioxide concentration across the mid-Pleistocene transition. Science, 324(5934), 1551–1554.

Ishikawa, T., Nagaishi, K., 2011. High-precision isotopic analysis of boron by positive thermal ionization mass spectrometry with sample preheating. J. Anal. Atom. Spectrom. 26(2), 359–365.

Ishikawa, T., Nakamura, E., 1990. Suppression of boron volatilization from a hydrofluoric acid solution using a boron-mannitol complex. Anal. Chem. 62(23), 2612–2616.

Ishikawa, T., Nakamura, E., 1993. Boron isotope systematics of marine sediments. Earth Planet. Sci. Let. 117, 567–580.

Komor, S. C., 1997. Boron contents and isotopic compositions of hog manure, selected fertilizers and water in Minnesota. J. Environ. Qual. 26, 1212–1222.

Kubota, K., Yokoyama, Y., Ishikawa, T., Obrochta, S., Suzuki, A., 2014. Larger CO_2 source at the equatorial Pacific during the last deglaciation. Sci. Rep. 4, 5261.

Kubota, K., Yokoyama, Y., Ishikawa, T., Suzuki, A., Ishii, M., 2017. Rapid decline in pH of coral calcification fluid due to incorporation of anthropogenic CO_2. Sci. Rep. 7, 7694.

Lea, D. W., Boyle, E. A., 1993. Determination of carbonate-bound barium in foraminifera and corals by isotope dilution plasma-mass spectrometry. Chem. Geol. 103(1-4), 73–84.

Lécuyer, C., Grandjean, P., Reynard, B., Albarède, F., Telouk, P., 2002. $^{11}B/^{10}B$ analysis of geological materials by ICP–MS Plasma 54: Application to the boron fractionation between brachiopod calcite and seawater. Chem. Geol. 186(1-2), 45–55.

Martinez-Boti, M. A., Marino, G., Foster, G. L., Ziveri, P., Henehan, M. J., Rae, J. W. B., Mortyn, P. G., Vance, D., 2015a. Boron isotope evidence for oceanic carbon dioxide leakage during the last deglaciation. Nature 518, 219–222.

Martínez-Botí, M. A., Foster, G. L., Chalk, T. B., Rohling, E. J., Sexton, P. F., Lunt, D. J., Pancost, R. D., Badger, M. P. S., Schmidt, D. N., 2015b. Plio-Pleistocene climate sensitivity evaluated using high-resolution CO_2 records. Nature 518, 49–54.

McCulloch, M. T., Holcomb, M., Rankenburg, K., Trotter, J. A., 2014. Rapid, high-precision measurements of boron isotopic compositions in marine carbonates. Rapid Commun. Mass Spectrom. 28(24), 2704–2712.

McCulloch, M., Falter, J., Trotter, J., Montagna, P., 2012. Coral resilience to ocean acidification and global warming through pH up-regulation. Nat. Clim. Change, 2(8), 623.

Nagaishi, K. and Ishikawa, T., 2009, A simple method for the precise determination of boron, zirconium, niobium, hafnium and tantalum using ICP-MS and new results for rock reference samples. Geochem. J., 43, 133-141.

Misra, S., Owen, R., Kerr, J., Greaves, M., Elderfield, H., 2014. Determination of $\delta^{11}B$ by HR- ICP-MS from mass limited samples: application to natural carbonates and water samples. Geochim. Cosmochim. Acta 140, 531–552.

Miyata, Y., Tokieda, T., Amakawa, H., Uematsu, M., Nozaki, Y., 2000. Boron isotope variations in the atmosphere. Tellus 52B (4), 1057–1065.

Nagaishi, K., and Tanimizu, M., 2012. Evaluation of accuracy and precision for boron isotope analysis using MC-ICPMS. Abstract for the Annual Meeting of The Geochemistry Society of Japan; Geochemical Society of Japan: Tokyo, 2012; https://dx.doi.org/10.14862/geochemproc.59.0.129.0.

Ni, Y., Foster, G. L., Elliott, T., 2010. The accuracy of δ^{11}B measurements of foraminifers. Chem. Geol. 274(3-4), 187–195.

Ni, Y., Foster, G. L., Bailey, T., Elliott, T., Schmidt, D. N., Pearson, P., Haley, B., Coath, C., 2007. A core top assessment of proxies for the ocean carbonate system in surface-dwelling foraminifers. Paleoceanogr. 22, PA3212, https://dx.doi.org/10.1029/2006PA001337.

Oda, H., Kawasaki, A., Hirata, T., 2001. Determination of the Geographic Origin of Brown-Rice with Isotope Ratios of ^{11}B/^{10}B and ^{87}Sr/^{86}Sr. Proceedings of IUPAC International Congress on Analytical Sciences 2001 (ICAS 2001), 17, 627–630.

Palmer, M. R., Pearson, P. N., 2003. A 23,000-Year Record of Surface Water pH and pCO$_2$ in the Western Equatorial Pacific Ocean. Science 300, 480–482.

Raitzsch, M., Bijma, J., Benthien, A., Richter, K. U., Steinhoefel, G., Kučera, M., 2018. Boron isotope-based seasonal paleo-pH reconstruction for the Southeast Atlantic–A multispecies approach using habitat preference of planktonic foraminifera. Earth Planet. Sci. Let. 487, 138–150.

Rosner, M., Romer, R. L., Meixner, A., 2005. Air handling in clean laboratory environments: the reason for anomalously high boron background levels. Anal. Bioanal. Chem. 382(1), 120–124.

Sagawa, T., Yokoyama, Y., Ikehara, M., Kuwae, M., 2012. Shoaling of the western equatorial Pacific thermocline during the last glacial maximum inferred from multispecies temperature reconstruction of planktonic foraminifera. Palaeogeogr. Palaeoclim. Palaeoecol. 346–347, 120–129.

Sakata, M., Natsumi, M., Tani, Y., 2010, Isotopic evidence of boron in precipitation originating from coal burning in Asian continent. Geochem. J., 44, 113–123.

Schlesinger, W. H., Vengosh, A., 2016. Global boron cycle in the Anthropocene, Glob. Biogeochem. Cyc. 30, 219–230, doi:10.1002/ 2015GB005266.

Sexton, P. F., Wilson, P. A., Pearson, P. N., 2006. Microstructural and geochemical perspectives on planktic foraminiferal preservation: “Glassy” versus “Frosty”. Geochem. Geophys. Geosys. 7(12), https://dx.doi.org./10.1029/2006GC001291.

Tanaka K., Holcomb M., Takahashi A., Kurihara H., Asami R., Shinjo R., Sowa K., Rankenburg K., Watanabe T. and McCulloch M., 2015. Response of *Acropora digitifera* to ocean acidification: constraints from δ^{11}B, Sr, Mg, and Ba compositions of aragonitic skeletons cultured under variable seawater pH. Coral Reefs 34(4), 1139–1149.

Tanimizu, M., Nagaishi, K., Ishikawa, T., 2018. A Rapid and Precise Determination of Boron Isotope Ratio in Water and Carbonate Samples by Multiple Collector ICP-MS. Anal. Sci. 34, 667–674.

de Villiers, S., Greaves, M., Elderfield, H., 2002. An intensity ratio calibration method for the accurate determination of Mg/Ca and Sr/Ca of marine carbonates by ICP□AES. Geochem. Geophys. Geosys. 3(1), https://dx.doi.org/10.1029/ 2001GC000169.

Wieser, M., Iyer, S., Krouse, H., Cantagallo, M., 2001. Variations in the isotope composition of *Coffea arabica* beans. Appl. Geochemistry 16, 317–322.

Wu, H. C., Dissard, D., Douville, E., Blamart, D., Bordier, L., Tribollet, A., Le Cornec, F., Pons-Branchu, E., Dapoigny, A., Lazareth, C. E., 2018. Surface ocean pH variations since 1689 CE and recent ocean acidification in the tropical South Pacific. Nat. Commun. 9(1), 2543.

Xiao, Y., Swihart, G. H., Xiao, Y., Vocke Jr, R. D., 2001. A preliminary experimental study of the boron concentration in vapor and the isotopic fractionation of boron between seawater and vapor during evaporation of seawater. Sci. China Ser. B 44 (5), 540–551.

Xu, Q., Dong, Y., Zhu, H., Sun, A., 2015. Separation and analysis of boron isotope in high plant by thermal ionization mass spectrometry. Int. J. Anal. Chem. https://doi.org/10.1155/2015/364242.

Yamaoka, K., Ishikawa, T., Matsubaya, O., Ishiyama, D., Nagaishi, K., Hiroyasu, Y., Chiba, H., and Kawahata, H., 2012, Boron and oxygen isotope systematics for a complete section of oceanic crustal rocks in the Oman ophiolite. Geochim. Cosmochim. Acta, 84, 543-559.

Yamazaki, T., Kanamatsu, T., Mizuno, S., Hokanishi, N., Gaffar, E. Z., 2008. Geomagnetic field variations during the last 400 kyr in the western equatorial Pacific: Paleointensity-inclination correlation revisited. Geophys. Res. Let. 35, L20307, https://dx.doi.org/10.1029/2008GL035373.

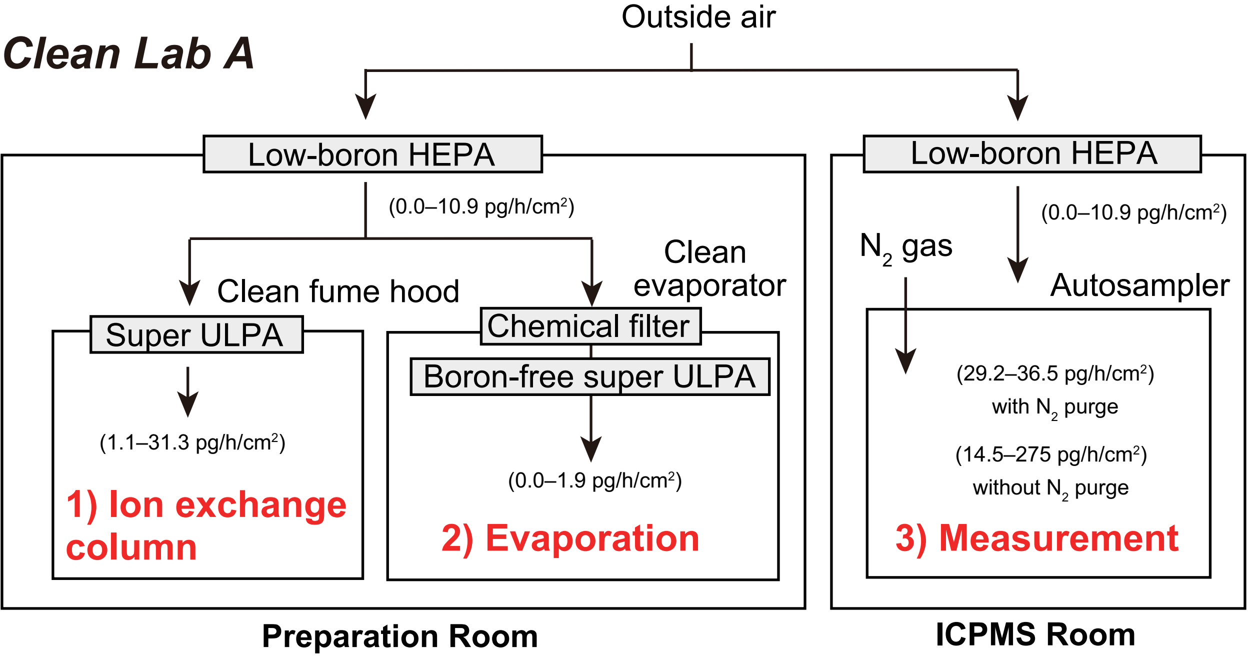
Clean Lab A
Outside air
Low-boron HEPA
(0.0–10.9 pg/h/cm²)
Clean fume hood
Clean evaporator
Super ULPA
(1.1–31.3 pg/h/cm²)
1) Ion exchange column
Chemical filter
Boron-free super ULPA
(0.0–1.9 pg/h/cm²)
2) Evaporation
Preparation Room
Low-boron HEPA
(0.0–10.9 pg/h/cm²)
N₂ gas
Autosampler
(29.2–36.5 pg/h/cm²) with N₂ purge
(14.5–275 pg/h/cm²) without N₂ purge
3) Measurement
ICPMS Room

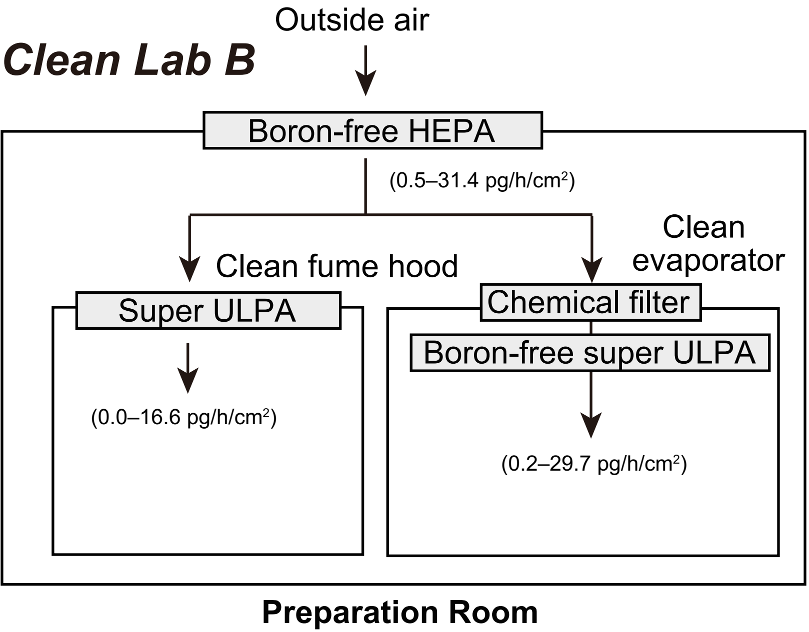
Clean Lab B
Outside air
Boron-free HEPA
(0.5–31.4 pg/h/cm²)
Clean fume hood
Clean evaporator
Super ULPA
(0.0–16.6 pg/h/cm²)
Chemical filter
Boron-free super ULPA
(0.2–29.7 pg/h/cm²)
Preparation Room

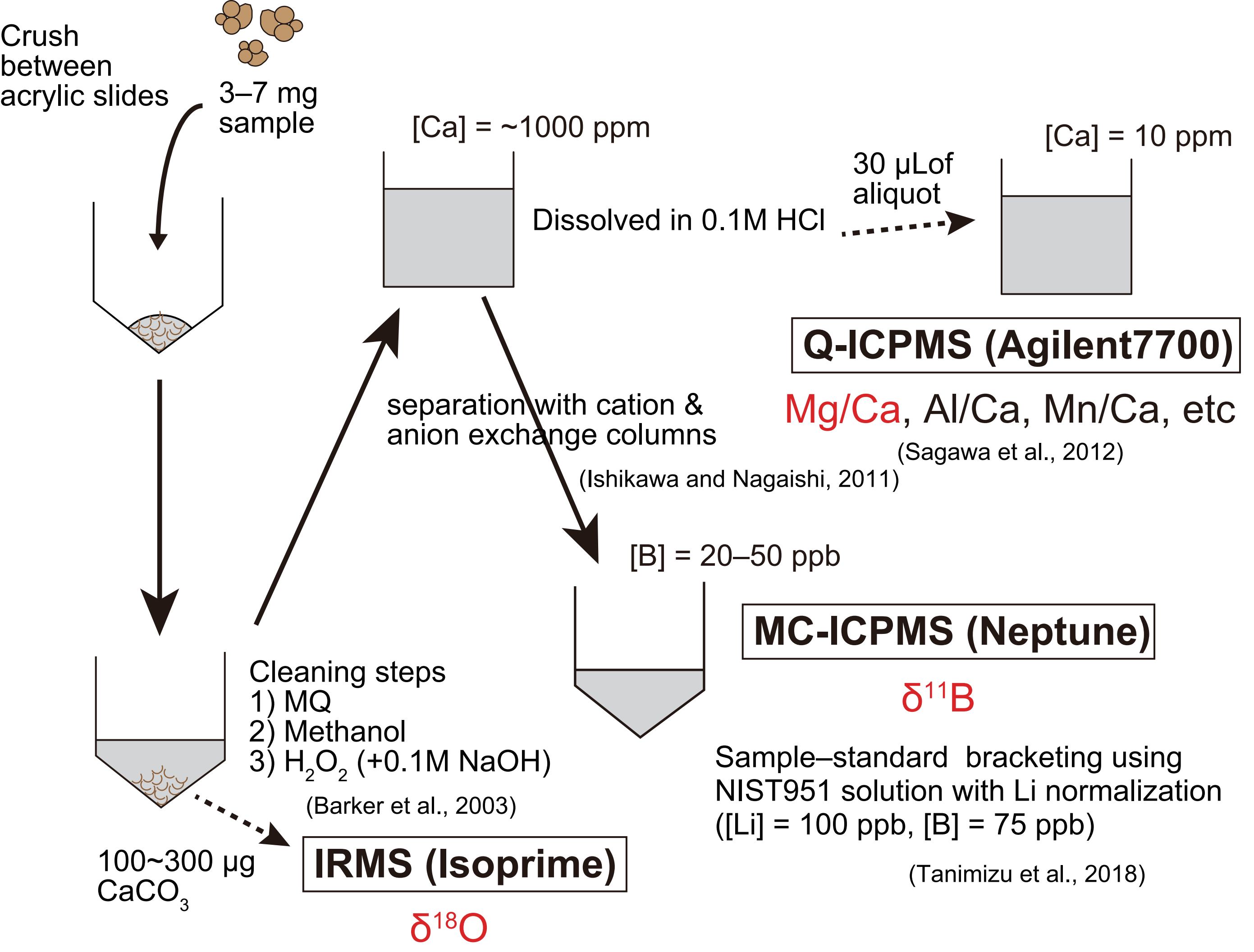
Crush between acrylic slides
3–7 mg sample
[Ca] = ~1000 ppm
Dissolved in 0.1M HCl
30 μLof aliquot
[Ca] = 10 ppm
Q-ICPMS (Agilent7700)
Mg/Ca, Al/Ca, Mn/Ca, etc
(Sagawa et al., 2012)
separation with cation & anion exchange columns
(Ishikawa and Nagaishi, 2011)
[B] = 20–50 ppb
MC-ICPMS (Neptune)
δ11B
Sample–standard bracketing using NIST951 solution with Li normalization ([Li] = 100 ppb, [B] = 75 ppb)
(Tanimizu et al., 2018)
Cleaning steps
1) MQ
2) Methanol
3) H2O2 (+0.1M NaOH)
(Barker et al., 2003)
100~300 μg CaCO3
IRMS (Isoprime)
δ18O

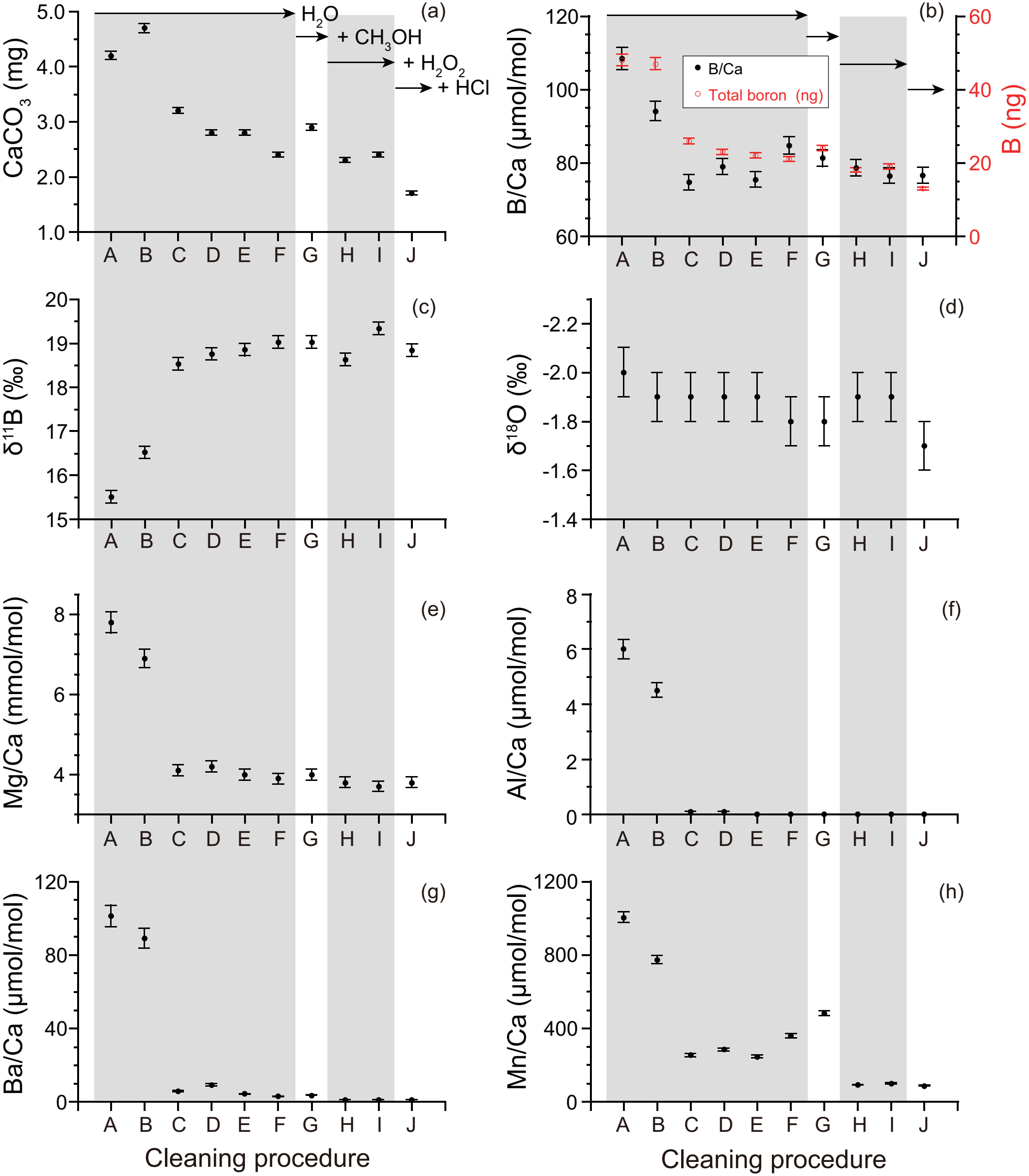
(a)
(b)
(c)
(d)
(e)
(f)
(g)
(h)
H$_2$O
+ CH$_3$OH
+ H$_2$O$_2$
+ HCl
CaCO$_3$ (mg)
1.0
2.0
3.0
4.0
5.0
B/Ca (μmol/mol)
60
80
100
120
B (ng)
0
20
40
60
● B/Ca
○ Total boron (ng)
δ^{11}B (‰)
15
16
17
18
19
20
δ^{18}O (‰)
-1.4
-1.6
-1.8
-2.0
-2.2
Mg/Ca (mmol/mol)
4
6
8
Al/Ca (μmol/mol)
0
2
4
6
8
Ba/Ca (μmol/mol)
0
40
80
120
Mn/Ca (μmol/mol)
0
400
800
1200
A
B
C
D
E
F
G
H
I
J
Cleaning procedure

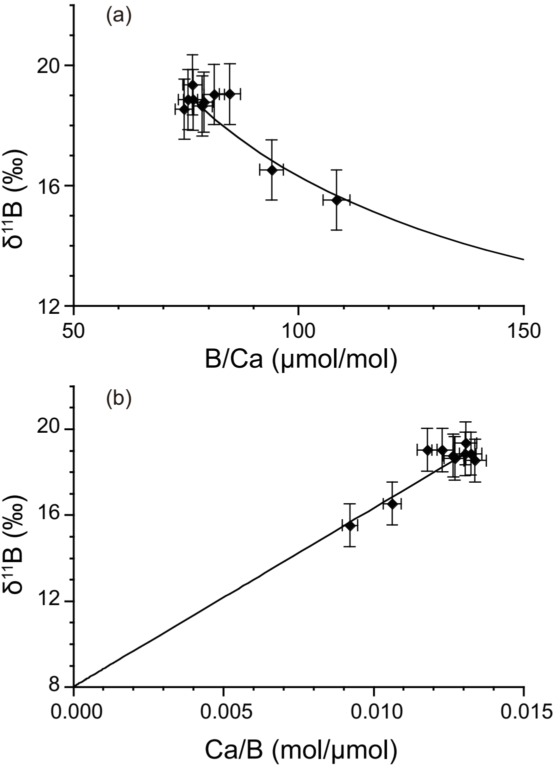
(a)
δ11B (‰)
20
16
12
50
100
150
B/Ca (μmol/mol)
(b)
δ11B (‰)
20
16
12
8
0.000
0.005
0.010
0.015
Ca/B (mol/μmol)

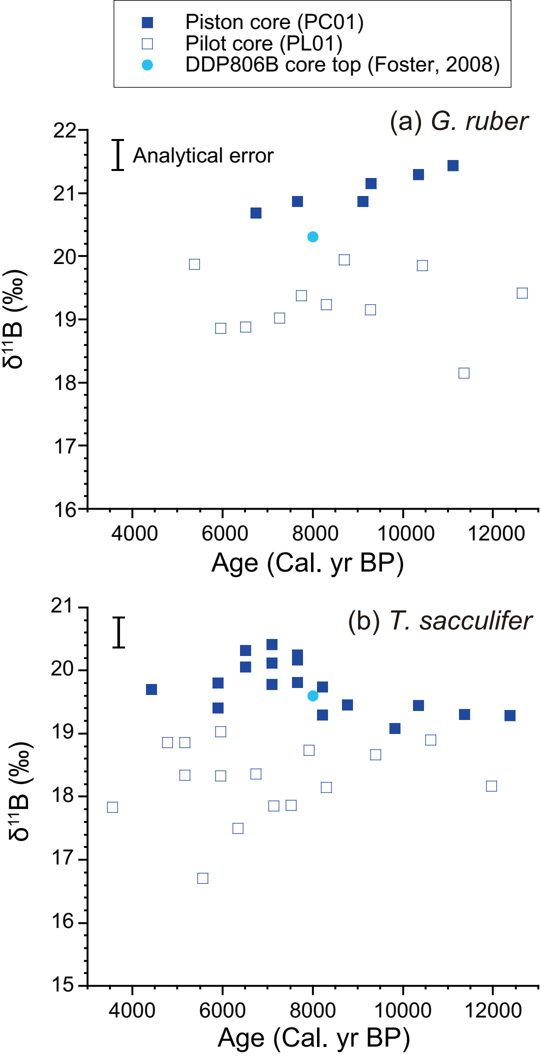
■ Piston core (PC01)
□ Pilot core (PL01)
● DDP806B core top (Foster, 2008)
(a) G. ruber
Analytical error
δ11B (‰)
22
21
20
19
18
17
16
4000
6000
8000
10000
12000
Age (Cal. yr BP)
(b) T. sacculifer
δ11B (‰)
21
20
19
18
17
16
15
4000
6000
8000
10000
12000
Age (Cal. yr BP)

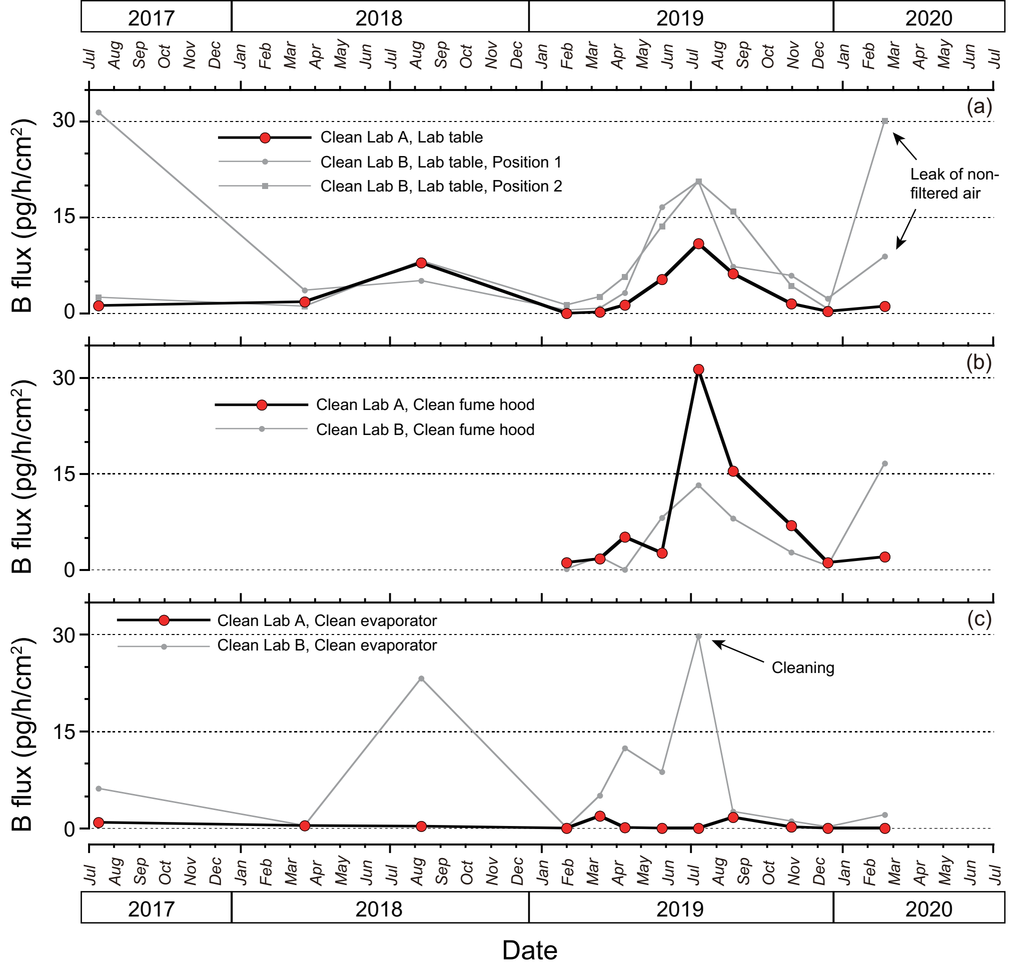
2017
2018
2019
2020
Jul Aug Sep Oct Nov Dec Jan Feb Mar Apr May Jun Jul Aug Sep Oct Nov Dec Jan Feb Mar Apr May Jun Jul Aug Sep Oct Nov Dec Jan Feb Mar Apr May Jun Jul
(a)
Clean Lab A, Lab table
Clean Lab B, Lab table, Position 1
Clean Lab B, Lab table, Position 2
Leak of non-filtered air
(b)
Clean Lab A, Clean fume hood
Clean Lab B, Clean fume hood
(c)
Clean Lab A, Clean evaporator
Clean Lab B, Clean evaporator
Cleaning
B flux (pg/h/cm^2)
0
15
30
Date

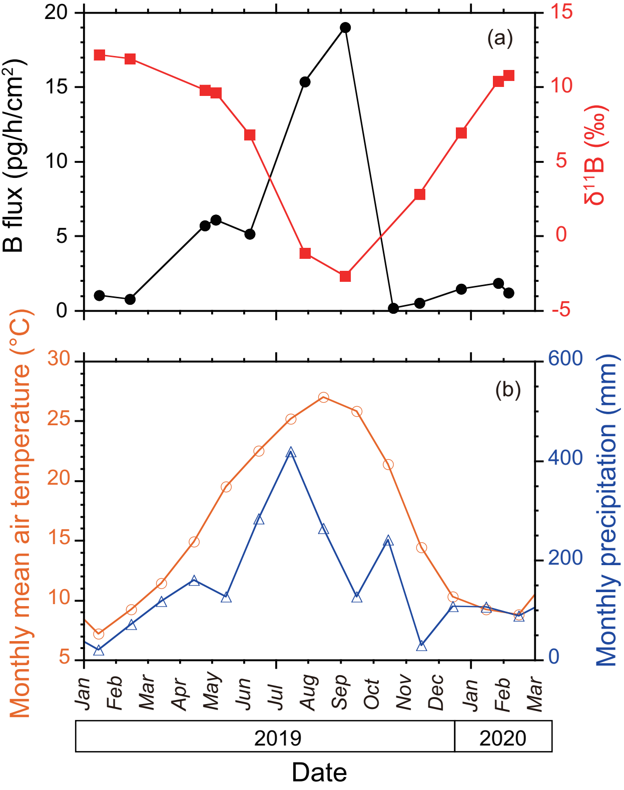
(a)
B flux (pg/h/cm^2)
20
15
10
5
0
$\delta^{11}B$ (‰)
15
10
5
0
-5
(b)
Monthly mean air temperature (°C)
30
25
20
15
10
5
Monthly precipitation (mm)
600
400
200
0
Jan
Feb
Mar
Apr
May
Jun
Jul
Aug
Sep
Oct
Nov
Dec
Jan
Feb
Mar
2019
2020
Date

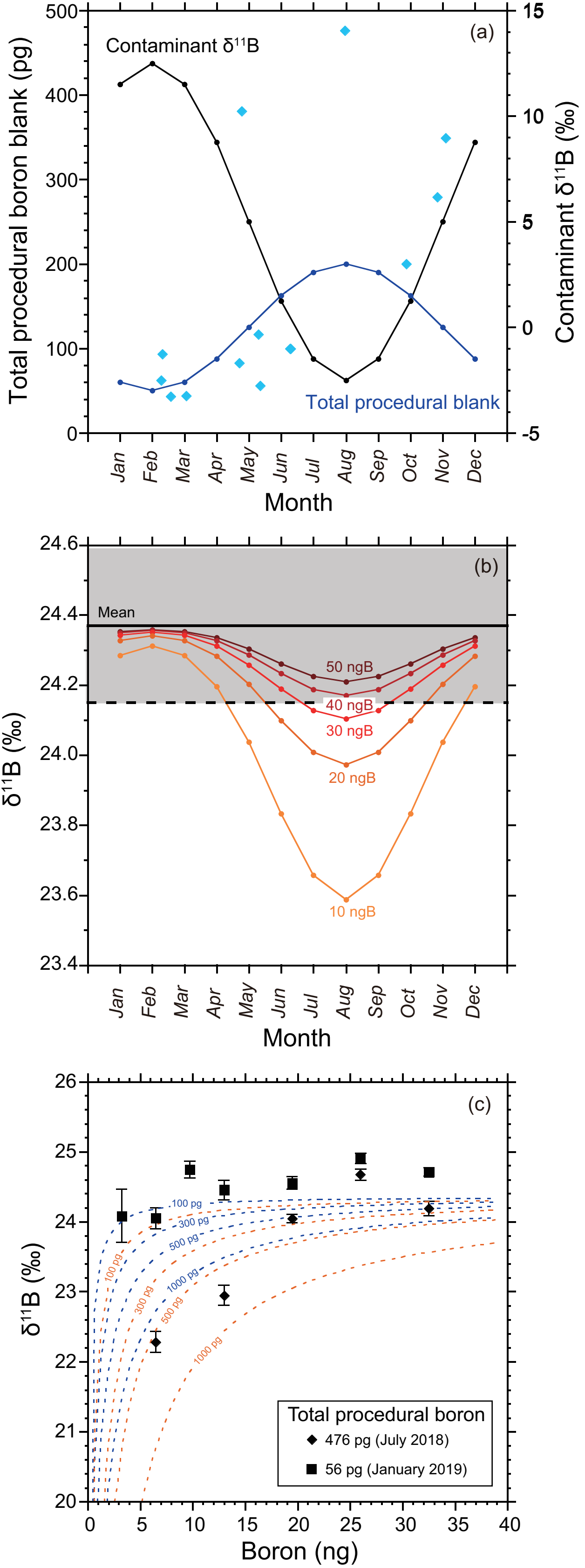
(a)
Contaminant δ11B
Total procedural blank
Total procedural boron blank (pg)
Contaminant δ11B (‰)
0
100
200
300
400
500
-5
0
5
10
15
Jan
Feb
Mar
Apr
May
Jun
Jul
Aug
Sep
Oct
Nov
Dec
Month
(b)
Mean
50 ngB
40 ngB
30 ngB
20 ngB
10 ngB
δ11B (‰)
23.4
23.6
23.8
24.0
24.2
24.4
24.6
Jan
Feb
Mar
Apr
May
Jun
Jul
Aug
Sep
Oct
Nov
Dec
Month
(c)
100 pg
300 pg
500 pg
1000 pg
100 pg
300 pg
500 pg
1000 pg
Total procedural boron
◆ 476 pg (July 2018)
■ 56 pg (January 2019)
δ11B (‰)
20
21
22
23
24
25
26
0
5
10
15
20
25
30
35
40
Boron (ng)

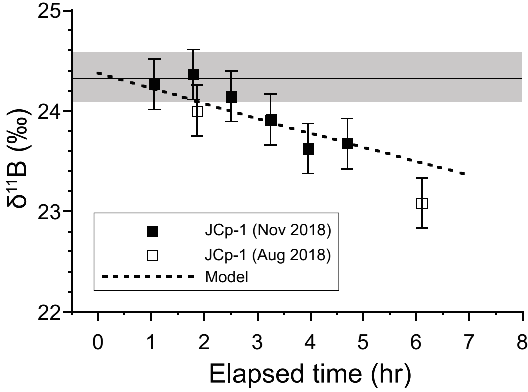
25
24
23
22
δ¹¹B (‰)
0
1
2
3
4
5
6
7
8
Elapsed time (hr)
JCp-1 (Nov 2018)
JCp-1 (Aug 2018)
Model

Table 1. Procedures for stepwise cleaning of foraminiferal shells. Numbers in columns represent replicates for each washing step.

Procedure	MQ H_2O	Methanol	Alkali-buffered H_2O_2	0.5 mM HCl
A	–	–	–	–
B	1	–	–	–
C	3	–	–	–
D	5	–	–	–
E	7	–	–	–
F	9	–	–	–
G	9	2	–	–
H	9	2	1	–
I	9	2	2	–
J	9	2	2	1